IOP Publishing
Measurement Science and Technology
Meas. Sci. Technol. **31** (2020) 052001 (15pp)
https://doi.org/10.1088/1361-6501/ab5f85

Topical Review

High spatial resolution: an integrative review of its developments on the Brillouin optical time- and correlation-domain analysis

Benzhang Wang[1], Yongkang Dong[1], Dexin Ba[1] and Xiaoyi Bao[2]

[1] National Key Laboratory of Science and Technology on Tunable Laser, Harbin Institute of Technology, Harbin 150001, People's Republic of China
[2] Fiber Optics Group, Department of Physics, University of Ottawa, Ottawa, Ontario K1N 6N5, Canada

E-mail: aldendong@163.com

Received 6 November 2018, revised 27 November 2019
Accepted for publication 6 December 2019
Published 31 January 2020

Abstract

In the past two decades, Brillouin-based optical fiber sensors have gained significant ground for distributed temperature and strain measurements in the real world. Among these sensors, Brillouin optical time-domain analysis (BOTDA) and Brillouin optical correlation-domain analysis (BOCDA) are good candidates to realize a high spatial resolution, which is of great importance to distinguish small-size events in practical applications. In this paper, high-spatial-resolution BOTDA and BOCDA are introduced and summarized. For the BOTDA, simulation experiments are made for further comprehension of the dark-pulse technique, pulse pre-pump (PPP) technique, differential pulse-width pair (DPP) technique and Brillouin echo technique. The dark-pulse and PPP techniques utilize the DC portion of the pulse signal, which brings the cross talk of the surrounding information. It is known as the non-local information in the Brillouin spectrum, which limits the minimum temperature and strain detection accuracy. The DPP and Brillouin echo techniques, utilizing differential measurement with two pump pulses, are free from this problem. The Brillouin echo-based sensor has a good signal-to-noise ratio, while the DPP-BOTDA owns the advantages of simple installation and easy implementation. For the BOCDA, its operating principle allows it to circumvent the pulse-based limit on the spatial resolution and two specific implementations are introduced, which are enabled by the frequency and phase modulation techniques. A brief overview of the developments and improvements on these two types of BOCDA sensor are introduced and summarized.

Keywords: high spatial resolution, stimulated Brillouin scattering, distributed optical fiber sensors

(Some figures may appear in colour only in the online journal)

1. Introduction

Stimulated Brillouin scattering (SBS)-based optical fiber sensors have become proven and applicable sensing schemes for temperature and strain measurements, due to the linear dependence of the fiber Brillouin frequency shift (BFS) on the strain and temperature variations [1]. The fiber works as a transmission and sensing element, providing a powerful mechanism for truly distributed strain and temperature measurements. After more than two decades of investigations and developments, the performance of the SBS-based sensors have been greatly enhanced in the aspect of measurement time [2], spatial resolution [3] and sensing range [4, 5]. Besides, the range of applications includes the fire alarming, pipeline leakage detection, structure health monitoring and so on [6]. Among these applications, the spatial resolution is a key property to distinguish the small-size events with distinct temperature/strain state. Therefore, much effort is made to improve the spatial resolution of the SBS-based sensors, especially for the Brillouin optical time-domain analysis (BOTDA) [3] and Brillouin optical correlation-domain analysis (BOCDA) [7].

In the BOTDA scheme, the pump wave is pulse modulated for distributed sensing, so that the spatial resolution is determined by the pulse width. The acoustic wave lifetime of 10 ns has imposed the pulse width limit for the associated spatial resolution to be 1 m [8]. The impacts of a short pulse (<10 ns) degrade the measurement accuracy, due to the broadened Brillouin spectrum and drastically reduced Brillouin interaction [8]. The first sub-meter spatial resolution in BOTDA has been demonstrated in 1998, where a spatial resolution of 50 cm is realized, enabled by a compound spectrum analysis method [9]. Otherwise, the detrimental effects induced by a short pulse can be mitigated with the DC leakage of the pulsed signal [10]. The DC portion acts as pre-pumping for short pulse-based BOTDA, which forms the foundation for the pre-pumping technique. Since then, more techniques have been proposed to realize a sub-meter spatial resolution at an acceptable measurement accuracy, including the dark-pulse technique [11], pulse pre-pump (PPP) technique [12], differential pulse-width (DPP) technique [13–15], Brillouin echo technique [16], Brillouin dynamic grating [17] and pulse subdivision analysis method [18].

In the BOCDA scheme, the SBS is localized at a specific position within the sensing fiber, due to the correlation between two modulated counter-propagating optical waves. There are several specific modulation methods to create the correlation peak, which are the frequency modulation [7], phase modulation [19], amplified spontaneous emission (ASE) [20] and chaotic laser [21]. The principle of the BOCDA allows it to circumvent the pulse-based spatial resolution limit, so that the spatial resolution can be obtained at the order of centimeters and even millimeters [22]. Moreover, further research is also conducted to enhance the BOCDA-based sensor performance, owning the capability of dynamic measurement [23], beyond one million sensing points [24] and so on.

In this paper, the main key techniques for the high-spatial-resolution BOTDA are introduced and summarized, and moreover some simulation experiments are made for further comprehension. Two main types of BOCDA (frequency modulation and phase modulation) are introduced and their developments are also summarized.

2. Operating principle

The SBS is a typical example of the stimulated light scattering resulting from the electrostriction effect, which introduces the refractive index variation (i.e. acoustic wave) by the action of an optical wave [26]. The acoustic wave is forward propagating with the pump wave, adding a Doppler shift to its backscattered Stokes wave, and the frequency shift (ν_B) is known as the BFS, given by [1, 2]:

$$\upsilon_B = \frac{2nV_a}{\lambda} \tag{1}$$

where n is the index of refraction, V_a is the velocity of the acoustic wave and λ is the light wavelength. For the wavelength of 1550 nm, the BFS of a conventional single-mode fiber is about 10.867 GHz [27]. When the counter-propagating probe wave is around the BFS relative to the pump wave, it will strengthen the acoustic wave by means of electrostriction. With the grown intensity of the acoustic wave, more pump wave is scattered and then the intensity of the probe wave is increased, so that the acoustic and probe waves mutually reinforce the intensity of each other. The above SBS process can be expressed by the coupled three-wave equations [25]:

$$\frac{\partial E_p}{\partial z} + \frac{n}{c}\frac{\partial E_p}{\partial t} = i\kappa E_s \rho \tag{2a}$$

$$-\frac{\partial E_s}{\partial z} + \frac{n}{c}\frac{\partial E_s}{\partial t} = i\kappa E_p \rho^* \tag{2b}$$

$$\frac{\partial \rho}{\partial t} + \left(\frac{1}{2}\Gamma_B + i(\Omega_B - \Omega)\right)\rho = i\Lambda E_p E_s^* \tag{2c}$$

where E_p, E_s and ρ are defined to be the field amplitudes of the pump wave, probe wave and the acoustic wave, respectively; Ω_B is the angular frequency of the BFS ($\Omega_B = 2\pi\nu_B$); Ω is the angular frequency offset between the pump and probe waves; Γ_B is the linewidth of the Brillouin gain spectrum (BGS); κ and Λ denote the elasto-optic and electrostrictive coupling coefficients, respectively. The fiber attenuation is ignored in the above equations for a short fiber length. Therefore, the accurate and general solutions of the coupled three-wave equations can be obtained by employing the numerical method with an implicit finite differencing in time and a down-winding or backward differencing in space [28]. The boundary conditions are known for the pump pulse at the beginning ($E_p(z,t)|_{z=0}$) and the probe wave at the far end ($E_s(z,t)|_{z=L}$).

After scanning the frequency offset between the pump and probe waves, the BGSs along the sensing fiber are measured. Then, the BFS can be obtained through the curve fitting method, the difference of which can be expressed by the following formula:

$$\Delta\nu_B = C_S\Delta\varepsilon + C_T\Delta T \tag{3}$$

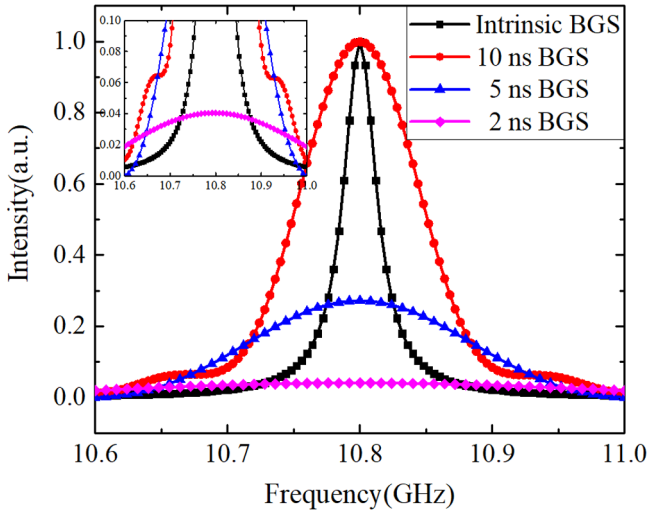

Figure 1. The influence of pulse width on the BGS profile.

where $\Delta\nu_B$ is the BFS difference; $\Delta\varepsilon$ is the strain variation and ΔT is the temperature variation; C_S and C_T denote the strain and temperature coefficients, respectively.

With the help of the numerical simulation, the influence of the pulse width on the BGS is investigated to verify the infeasibility of a short pulse for a high-spatial resolution. The Brillouin spectra of three different pulse widths (10 ns, 5 ns and 2 ns) are shown in figure 1, and the intrinsic BGS with a 30 MHz spectral width is also provided. It can be seen that the spectrum is broadened and the intensity is drastically reduced when pulse width decreases. As analysed by Soto and Thévenaz, the BFS accuracy can be expressed as follows [29]:

$$\sigma(z) = \frac{1}{\mathrm{SNR}(z)}\sqrt{\frac{3\cdot\delta\cdot\Delta\nu_B}{8\sqrt{2}(1-\eta)^{3/2}}} \tag{4}$$

where z denotes the location along the fiber under test (FUT); δ is the frequency sampling step, which is 2 MHz for all the simulation experiments in this paper; $\Delta\nu_B$ is the full width at half maximum (FWHM) of the BGS and η is the fraction of the peak level where a quadratic least-square fitting is employed. Besides, the 2 ns BGS is also shown in detail in the inset figure, which indicates that the measurement accuracy will be seriously deteriorated due to the low signal-to-noise ratio (SNR) and wide spectrum. Here, the value of main simulation parameters are listed: $c = 3\times10^8$ m s^{-1} is the light velocity in vacuum; $n = 1.5$ is the refractive index of the fiber; $\Gamma_B = 2\pi\Delta\nu_B = 2\pi\cdot30$ MHz is the linewidth of the intrinsic BGS; $L = 10$ m is the length of FUT; $\nu_B = 10.800$ GHz is the stress-free BFS of the FUT at ambient temperature. In the sections 3 and 4, the novel techniques for the high-spatial-resolution BOTDA and BOCDA are introduced and summarized.

3. The developments of high-spatial-resolution BOTDA

For the BOTDA sensors, it is unpractical to obtain a sub-meter spatial resolution with an optical pulse of less than 5 ns. In 1999, a sub-meter spatial resolution was obtained by the pre-excitation of the acoustic wave, while the width of the Brillouin spectrum is maintained at its natural value, which offers a new way to exploit the high-spatial-resolution BOTDA sensors [8]. Based on this powerful operating principle, several impressive techniques have been developed, including the dark-pulse technique, PPP technique, DPP technique and Brillouin echo technique. In figure 2, the detailed pulse modulation on the pump wave is shown for each technique. In the dark-pulse and PPP schemes, the spatial resolution is determined by the width of the short pulse (Δt). In the other two schemes, a high spatial resolution is enabled by using two pump pulses with a slight difference (Δt) on width or phase.

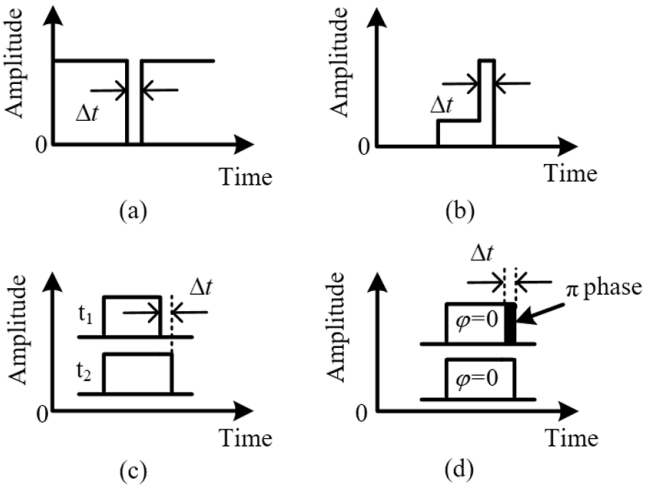

Figure 2. Four main techniques and the corresponding pulse modulation methods: (a) dark-pulse technique; (b) PPP technique; (c) DPP technique; and (d) Brillouin echo technique.

3.1. Dark-pulse-technique-based BOTDA

The dark-pulse technique has been proposed by Brown *et al* in 2005 [11], which is able to achieve a high spatial resolution and overcome the above two obstacles (i.e. broadened spectrum and reduced intensity). In the experiment, the system is working in the Brillouin loss scheme. The anti-Stokes wave is a continuous wave (CW), while the pump wave is dark pulse modulated as a quasi-CW as shown in figure 2(a). Adjusting the bias voltage of the Mach–Zehnder modulator (MZM) at its maximum transmission, the dark pulse can be generated with an electrical pulse. The CW component of pump and anti-Stokes wave will excite the acoustic wave, and the power is continuously transferred from the anti-Stokes wave to the pump wave. When the dark pulse injecting into the fiber, the interaction is switched off during the pulse width, resulting in a power increasement on the anti-Stokes wave. Moreover, the intensity of the acoustic wave will not be much changed, as the pulse width is much shorter than the acoustic wave lifetime. So the linewidth of the measured BGS is equal to its natural value, which is able to maintain a high measurement accuracy. As a result, it is able to realize a 5 cm spatial resolution over a 100 m sensing fiber [11]. Furthermore, in 2007,

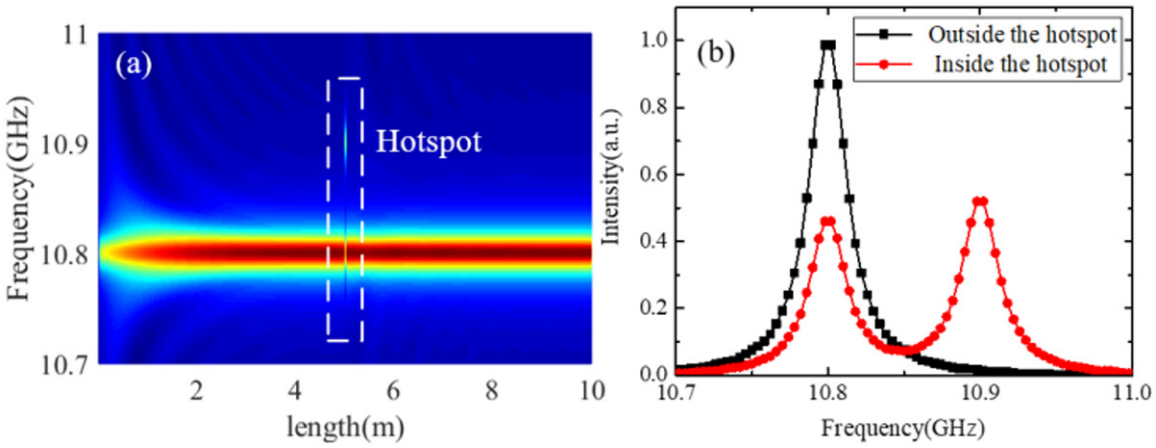

Figure 3. (a) The 3D BGSs of the dark-pulse-based BOTDA along the FUT, and (b) the BGSs inside and outside the hotspot.

the spatial resolution is optimized to 2 cm with a 200 ps dark pulse [30].

Next, a simulation experiment is made to further investigate the dark-pulse-technique-based BOTDA, which is operated in the Brillouin gain scheme. The general simulation parameters are the same as used in section 2, and the main difference is the boundary condition of the pump wave:

$$E_{\mathrm{p}}(z,t)|_{z=0} = \begin{cases} 0 & T \leqslant t \leqslant T+\Delta t \\ \sqrt{\frac{P_{\mathrm{p}}}{A_{\mathrm{eff}}}} & \text{else} \end{cases} \tag{5}$$

where $P_{\mathrm{p}} = 4$ mW is the power of the pump wave; $\Delta t = 0.2$ ns is the width of dark pulse; $A_{\mathrm{eff}} = 50\ \mu\mathrm{m}^2$ is the effective core area. Besides, the power of the CW Stokes is chosen to be 0.1 mW.

In order to demonstrate the sensor capability of 2 cm spatial resolution, a 2 cm hotspot with a BFS of 10.900 GHz is centered at the location of 5 m. The simulated three-dimensional (3D) BGSs are shown in figure 3(a), where the hotspot is located in the middle with a 100 MHz frequency shift. The detailed BGSs inside and outside the hotspot are shown in figure 3(b), corresponding to the position of 5 m and 4.5 m, respectively. The FWHM of the simulated BGS is about 30 MHz, which is equal to its natural value. Therefore, the dark-pulse-technique-based BOTDA allows a high spatial resolution with no spectral broadening. However, the residual peak at 10.800 GHz is observed for the spectrum inside the hotspot, which is also measured in the experiment by Brown *et al* [30]. In their paper, it is explained as the relaxation of the acoustic wave after the passage of the pulse. Here, we think it is induced by the recovery of the acoustic wave where the dark pulse has been passed by. It is similar to the unwanted presence of the second echo using the Brillouin echo technique [16], which will also be introduced in the following part. Let us analyze this process under the following condition that the frequency offset between the pump and probe waves is near the fiber BFS at the ambient temperature. When the dark pulse enters into the FUT, it has a quenching influence on the acoustic wave, and then the subsequent pump wave and probe wave will re-strengthen the acoustic wave. Next, the dark pulse travels in the uniform fiber, and the energy transferred from the pump wave to the probe wave is stable, because there is a dynamic balance between the growing and decaying of the acoustic wave. When the dark pulse enters into the hotspot, the quenching effect on the acoustic wave becomes weak and even disappears as the resonance frequency is not satisfied inside the hotspot. On the whole, the balance is broken and the recovery of acoustic wave plays a dominant role, resulting in a slow increase on the probe intensity. Therefore, the residual peak is measured inside the hotspot, and it will exist for a while until the acoustic wave is returned to normal.

To exhibit the vanishing process of the residual peak, the length of the hotspot is increased to 4 m, and the simulated 3D BGSs are shown in figure 4(a). At the position between 5 m and 6 m, the residual peak at 10.800 GHz is fading away as a function of time. It can be regarded as a transient state (the recovery of the acoustic wave) and three typical BGSs in this case are shown in figure 4(b). In the steady state, the residual peak at 10.800 GHz is almost vanished at the position between 7 m and 9 m, as shown in figure 4(c). Due to the non-local response of the sensor, it is hard to distinguish a small BFS variation in a small-size hotspot.

Another simulation experiment is carried out to display the influence of residual peak on the BFS extraction, which is shown in figure 5. A 2 cm hotspot is measured with a 0.2 ns dark pulse, and the BFS difference is selected in three different values (30 MHz, 50 MHz and 100 MHz). It can be seen that the two peaks are easy to distinguish under the condition of 100 MHz, but they are very close under the condition of 30 MHz, bringing the difficulty to extract the BFS. As a result, the dark-pulse-based Brillouin sensing can be only used for a high-spatial-resolution measurement when the BFS difference between the hotspot and rest fiber is bigger than the linewidth of the intrinsic BGS. Moreover, the sensing length is also limited to kilometer scale, in case of the onset of the SBS [30].

3.2. Pulse pre-pump-technique-based BOTDA

The presence of a low-power DC leakage light is also able to pre-excite the acoustic wave before the arrival of the bright pulse [8, 31]. However, the measured BGS of a short fiber section is distorted if the strain or temperature is small. The underestimation of the strain or temperature caused by the

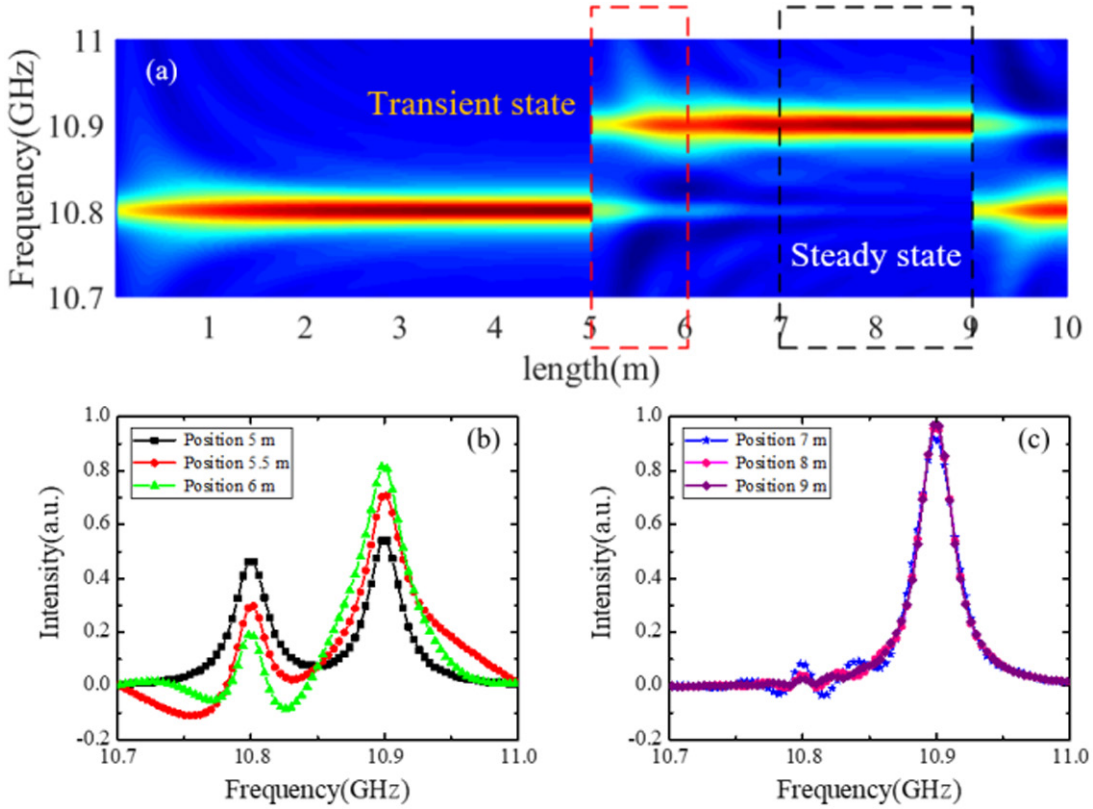

Figure 4. The detailed BGSs of the dark-pulse-based BOTDA for a 4 m hotspot: (a) the 3D BGSs along the 10 m FUT; (b) the typical BGSs in the transient state between 5 m and 6 m; and (c) the typical BGSs in the steady state between 7 m and 9 m.

pulse base is theoretically analyzed and experimentally demonstrated [32]. The schematic diagrams of the BOTDA using the pump pulse with DC leakage light is shown in figure 6(a), where E_p, C_p and E_{cw} denotes the field amplitudes of the pump pulse, DC leakage light and probe wave, respectively. In the system of figure 6(a), the process of interaction between a pump pulse with a DC leakage light (i.e. pulse base) and a CW probe wave in the FUT can be divided into four parts [33], as shown in table 1, according to which part of pump wave (bright pulse or pulse base) interacts with the probe wave through the acoustic wave excited by whichever part of the pump wave. Besides, the characteristic of each part is also summarized in table 1.

Part (1) is the traditional term in the BOTDA by using a short pulse, which enables the distributed measurements with a high spatial resolution and wide Brillouin spectrum (i.e. poor BFS resolution). Part (2) is the fundamental principle to obtain a high spatial resolution by pre-exciting the acoustic wave, as proved in [8, 31]. However, part (4) is the main reason for the underestimation of the strain and temperature, which distorts the BGS by the non-local Brillouin interaction. Moreover, the sensing range is also limited by part (4), due to the pump depletion and the Brillouin threshold.

To reduce the pulse base contribution on the BGS and maintain the useful component of part (2), a novel PPP-BOTDA has been proposed [12], and a schematic diagram is shown in figure 6(b). A spatial resolution of 10 cm is achieved with a 13 ns pre-pump pulse and a 1 ns pump pulse [33]. In 2008,

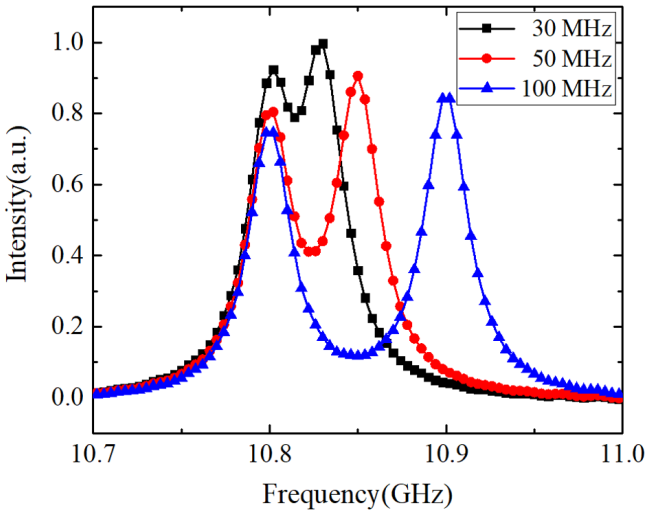

Figure 5. The influence of residual peak on BFS measurement in the dark-pulse-based BOTDA.

a pump pulse of a finite extinction ratio followed by a dark base of a finite length is also proposed to obtain a high spatial and frequency resolution [34]. Both of the above methods are proposed to reduce the intensity of part (4), so that the BFS of a small stress or temperature section can be determined at a lower peak value. Besides, the pump depletion is mitigated and the Brillouin threshold is increased, so that the sensing range can be extended.

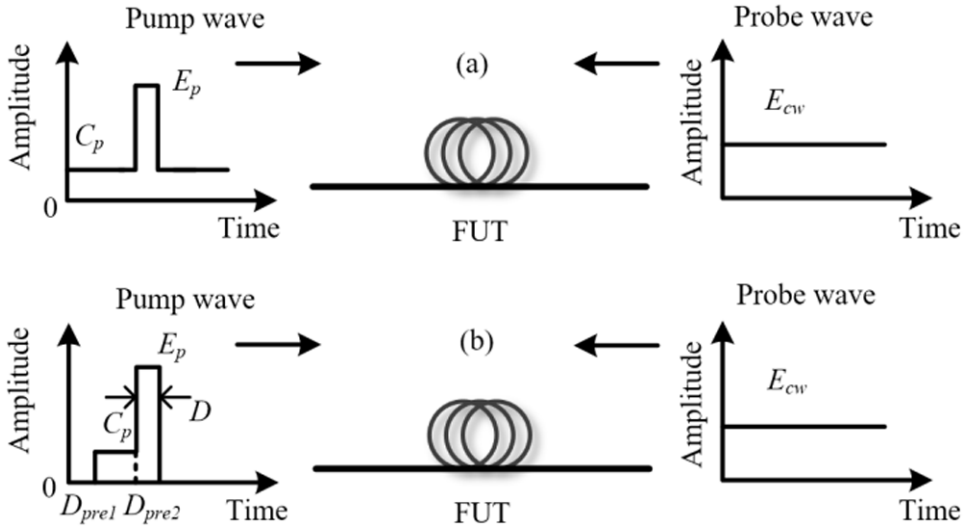

Figure 6. Schematic diagrams of (a) the pump pulse with a DC leakage light, and (b) the PPP-BOTDA.

Table 1. The interaction and characteristic of the four parts between a pump pulse with a pulse base and a CW probe wave.

Part	Part of the pump wave to interact with the probe wave	Part of the pump wave to excite the acoustic wave	Characteristic
1	Bright pulse	Bright pulse	High spatial resolution and wide Brillouin spectrum
2	Bright pulse	Pulse base	High spatial resolution and narrow Brillouin spectrum
3	Pulse base	Bright pulse	Vibration noise and complicate contents
4	Pulse base	Pulse base	No spatial resolution and narrow Brillouin spectrum

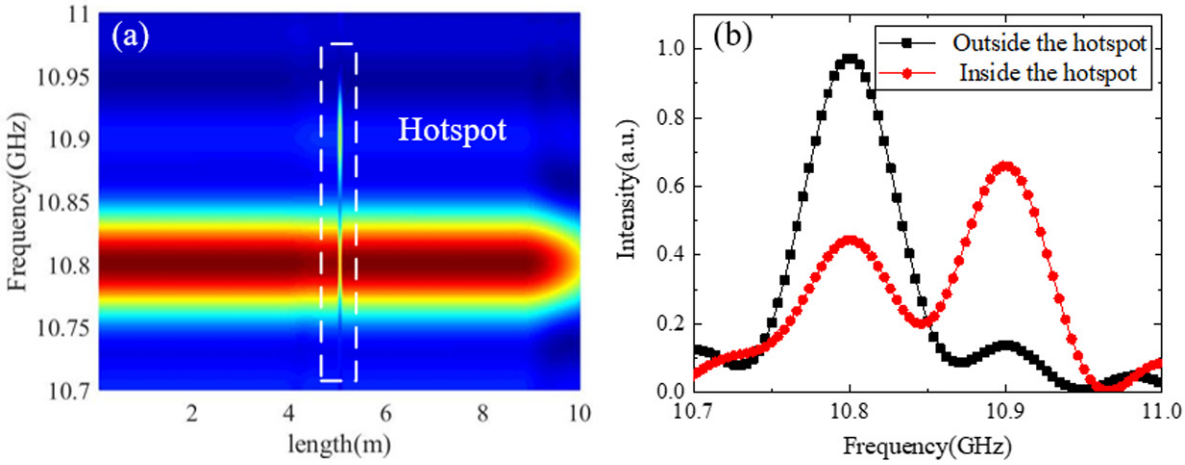

Figure 7. (a) The 3D BGSs of the PPP-BOTDA along the FUT, and (b) the BGSs inside and outside the hotspot.

The PPP-BOTDA is taken as a typical example for further investigation and the BGSs of the PPP-BOTDA are also obtained using the numerical simulation. The initial condition for pump pulse can be described as follows:

$$E_p(z,t)|_{z=0} = \begin{cases} C_\mathrm{p} & D_\mathrm{pre1} \leqslant t \leqslant D_\mathrm{pre2} \\ E_\mathrm{p} & D_\mathrm{pre2} \leqslant t \leqslant D_\mathrm{pre2} + D \\ 0 & \text{else} \end{cases} \tag{6}$$

where the peak power of the pump pulse is 100 mW; $D_\mathrm{pre} = D_\mathrm{pre2} - D_\mathrm{pre1} = 12$ ns is the width of the pre-pump pulse; $D = 0.5$ ns is the pump pulse width and the extinction ratio is about 13 dB, defined as $E_\mathrm{p}/C_\mathrm{p}$. Note that the value of the pre-pump pulse width and extinction ratio should be chosen carefully to guarantee the pre-excitation of the acoustic and avoid introducing excessive non-local information into the BGS.

The simulation results of the 3D BGSs are shown in figure 7(a), where a 5 cm hotspot is located in the middle with 100 MHz BFS difference. The power of the pump pulse is 100 mW (0.5 mW for the pre-pump pulse), while it is 0.1 mW for the probe wave. In figure 7(b), the BGSs inside and outside

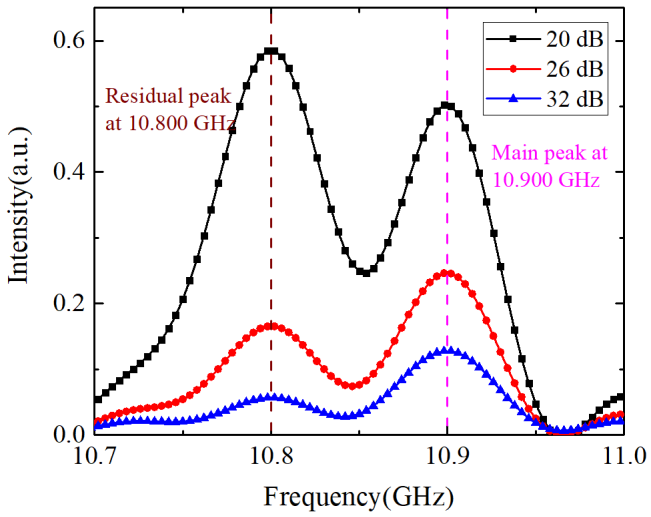

Figure 8. The influence of power extinction ratio on the BGS inside the hotspot.

the hotspot are presented, which proves that a spatial resolution of 5 cm is obtained by using the PPP technique. Besides, the FWHM of the measured BGS is about 105 MHz, which is narrowed by pre-exciting the acoustic wave. However, the residual peak and some fluctuations are introduced to the BGS, which can be explained by part (4) and part (1) in table 1. The center frequency of the main peak is about 10.7998 GHz and 10.8991 GHz for the BGSs inside and outside the hotspot, respectively. Compared with the true values (10.800 GHz and 10.900 GHz), a system measurement error about 0.9 MHz is induced by the distorted BGS.

Furthermore, another simulation experiment is carried out to display the influence of power extinction ratio ($(E_p/C_p)^2$) on the measurement, which is shown in figure 8. Note that the peak power of the pump pulse is fixed at 100 mW, while the peak power of the pre-pump pulse is about 1 mW, 0.25 mW and 62.5 μW, so that power extinction ratio is computed to be 20 dB, 26 dB and 32 dB, respectively. A low power extinction ratio means a strong pre-excited acoustic wave, resulting in a high SNR, but it will introduce excessive non-local information. As proved in the case of 20 dB, the intensity of the residual peak at 10.800 GHz is higher than that of the main peak at 10.900 GHz. When the power extinction ratio is increased to 32 dB, the intensity of the residual peak is lower than that of the main peak, and meanwhile the intensity of the whole signal is also reduced, degrading the sensor SNR. In the same vein, the width of the pre-pump pulse should also be optimized to introduce less non-local information at an acceptable SNR. As a result, the PPP-BOTDA is able to realize a sub-meter spatial resolution with a narrow Brillouin spectrum, but a system measurement error is also introduced by the non-local response of the sensor. In order to eliminate the detrimental effect induced by the pre-excitation pulse, the differential process has been introduced by subtracting between the BGSs with and without the main pulse (short pulse). This technique is learned from the DPP-BOTDA, which will be discussed in the next part [35].

3.3. Differential pulse-width-technique-based BOTDA

In 2008, the DPP technique has been proposed for a high-spatial-resolution measurement, which is known as the DPP-BOTDA. In the DPP-BOTDA scheme, two long duration pulses are used for two separate measurements and the differential Brillouin signal is obtained by making a subtraction between the two pulse-width signals [13]. The width of the differential BGS is determined by the long duration pulses, which can provide a good frequency resolution. The spatial resolution is determined by the difference between two pulse widths, and meanwhile the minimum effective spatial resolution is limited by the falling time of the optical pulse. The subtraction process can be also made in the optical domain before the photodetector, which utilizes the coherent interaction of the Brillouin gain and loss via optical differential parametric amplification [36]. In 2012, an upgraded DPP-BOTDA has been reported to work in the transient domain to decrease the reduction of the SNR after the differential process. Using the 8/8.2 ns pulse-width pair with a 150 ps falling time, it is able to achieve a 2 cm spatial resolution over a 2 km sensing fiber [14]. In 2017, the DPP-BOTDA is combined with a novel scanning method [37], which is able to increase the sensing range by avoiding the detrimental temporal distortion of the pump pulse. In the experiment, the performance is further enhanced to resolve one million sensing points, i.e. 1 cm spatial resolution over a 10 km single-mode fiber [15]. Moreover, the double peak spectrum is used to enhance the DPP-BOTDA capability of small event detection. A 5 cm hotspot at the far end of 24 km FUT has been measured by employing a 50 cm spatial resolution DPP-BOTDA, and the sampling rate is only 1 GS/s (corresponding to 10 cm/point). This technique is simple and cost-effective, which allows the DPP-BOTDA for higher spatial resolution measurements [3].

A simulation experiment is made to investigate the DPP-BOTDA performance on the high spatial resolution. A 1 cm hotspot is located in the middle of 10 m FUT, which is interrogated with a 10/10.1 ns pulse-width pair. The power of the pump pulse is 100 mW, while it is 0.1 mW for the probe wave. The Brillouin time traces at the 10.800 GHz are shown in figure 9, where the black curve and red curve are corresponding to the 10 ns and 10.1 ns signals, respectively. It can be seen that the rising time of the two long pump pulses is equal to the pulse width, resulting in a low spatial resolution. After subtracting between the two pulse-width Brillouin signals, the differential signal is obtained with a short rising time, as the same part of the rising edge is eliminated. As a result, the hotspot of 1 cm is clearly observed and located after the differential process, and then the 3D BGSs of the DPP-BOTDA are shown in figure 10(a). The BGSs inside and outside the hotspot are presented in figure 10(b), while the center frequency is the same as the natural value (10.800 GHz and 10.900 GHz). Besides, the FWHM of the measured BGS is about 95 MHz, which is determined by the long duration pulses. Note that the side lobe is attributed to the pump contribution on the Brillouin spectrum, i.e. the hidden peak of the 10 ns BGS in figure 1, which becomes more obvious after the differential process [14].

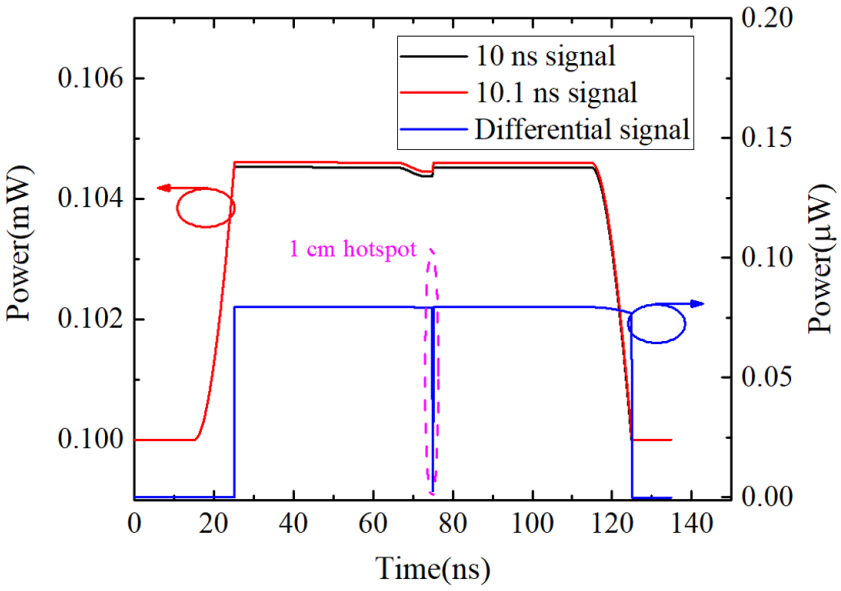

Figure 9. The Brillouin time traces of the 10 ns (black curve), 10.1 ns (red curve) and after the differential process (blue curve) at the frequency offset of 10.800 GHz.

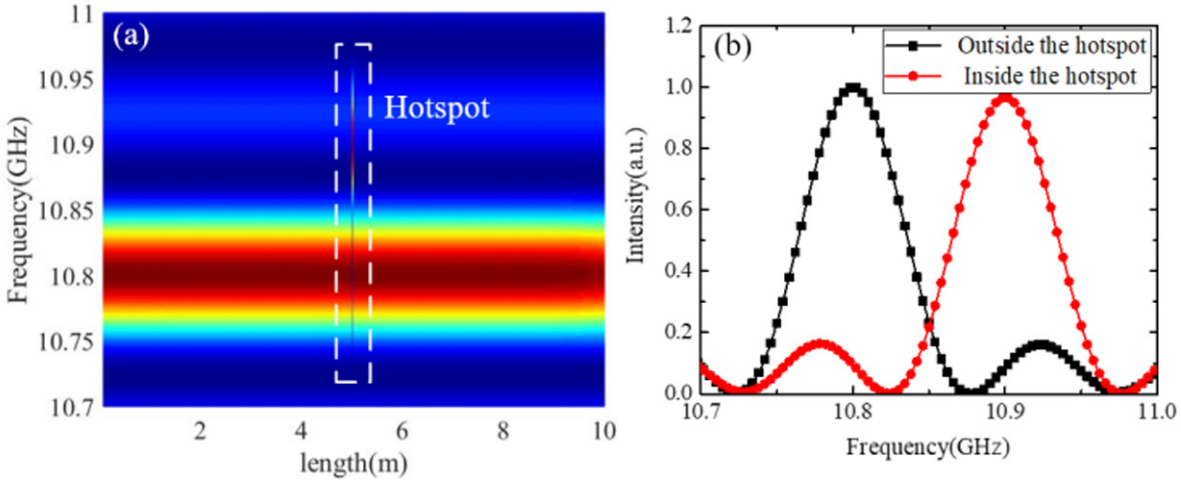

Figure 10. (a) The 3D BGSs of the DPP-BOTDA along the FUT, and (b) the BGSs inside and outside the hotspot.

The differential process is also an effective tool to enhance the measurement accuracy in the long-range Brillouin sensing [38]. After a long-range SBS interaction, the rising edge of output pulse is smoothed, due to the excitation time of the acoustic wave [39]. Then, an asymmetrical broadening is introduced to the pulse spectrum, resulting in a BFS measurement error [40]. Nevertheless, this BFS measurement error can be avoided by the DPP technique, as the measurement result is just the differential part of the pulse pair. As a result, the DPP-BOTDA is able to realize a high spatial and BFS resolution, and moreover the DPP technique has also been reported to reduce the pulse distortion induced measurement error in the long-range Brillouin sensing.

3.4. Brillouin echo distributed sensing

The Brillouin echo distributed sensing (BEDS) has been proposed for a high-spatial-resolution time-domain Brillouin

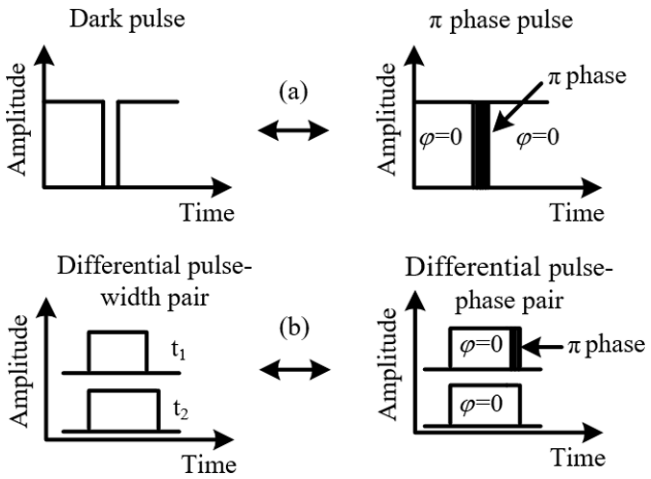

Figure 11. Comparison of the BEDS with the dark-pulse and DPP technique: (a) dark pulse and π phase pulse, and (b) DPP and differential pulse-phase pair.

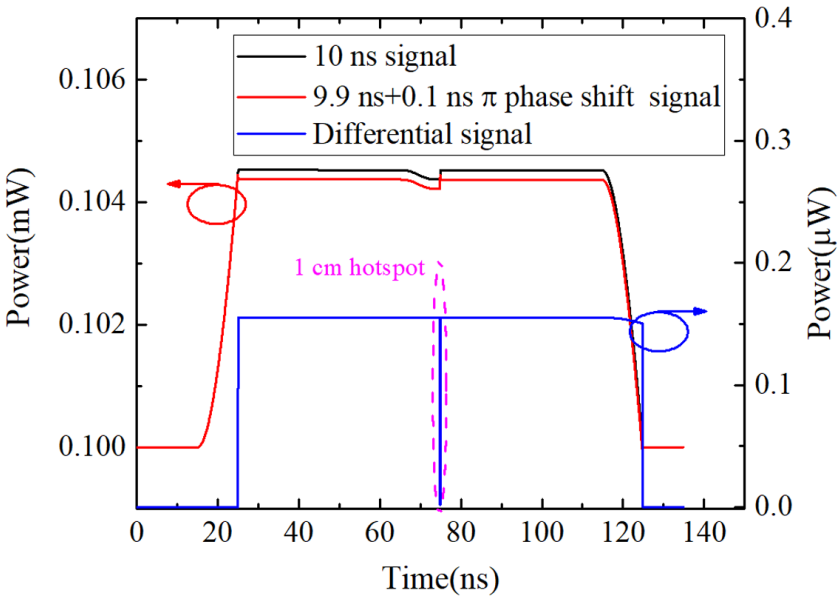

Figure 12. The Brillouin time traces of the 10 ns (black curve), 9.9 ns with 0.1 ns π phase pulse (red curve) and after the differential process (blue curve) at the frequency offset of 10.800 GHz.

measurement, which uses a π phase modulated pump pulse [16, 41]. Compared with the dark-pulse technique, the pump is π phase modulated, as shown in figure 11(a). Similarly, the acoustic wave is pre-excited by the no-phase shift pump wave, leading to a narrow Brillouin spectrum. When the π phase pulse injects into the FUT, the intensity of the SBS interaction is decreased by an out-of-phase quenching effect on the acoustic wave. When the π phase pulse has been passed (i.e. the phase shift returns to zero again), the acoustic wave will gradually recover. Since this type of interaction is similar to the 'spin-echoes' among the concepts of nuclear magnetic resonance, it is called BEDS for the similarity [41]. The spatial resolution is determined by the width of π phase pulse, and the π phase pulse can be obtained with a phase modulator [16, 41].

Due to the recovery of the acoustic wave, the non-local information is also introduced as the residual peak inside and after the hotspot, which is named the second echo in their work. In order to overcome the detrimental effect of the second echo, the pump wave after the phase pulse should be extinguished, so that the recovery of the acoustic wave is avoided. In practice, the pump wave is pulse modulated with an intensity modulator as shown in figure 11(b). Then, a phase modulator is followed for the π phase shift modulation. The pulse width is recommended to be long enough (~30 ns) to fully excite the acoustic wave. Ultimately, the most important is how to extract the contribution of the short π phase pulse. In 2008, for the first time, the differential pulse-phase pair technique has been proposed to achieve this goal [41]. In the other measurement, the pump wave is only pulse modulated with no phase modulation, as the other pulse in figure 11(b). In order to compare with the DPP-BOTDA, the response of these two differential techniques is made, and the result shows that the phase pulse optimizes the response by improving the contrast by a factor of 2 [16]. It indicates that the BEDS owns the capability of a higher SNR, which can provide a better measurement accuracy under the same conditions. In terms of the performance, it is able to achieve a 10 cm spatial resolution in 2008 [41], and a better result of 5 cm spatial resolution over 5 km sensing fiber is obtained in 2010 [16]. The differential phase-shift-keying technique is also introduced to the BEDS. It is able to generate a normal pump pulse and a π phase shift pump pulse with a single MZM, and the adjustment of the phase delay is easy and accurate [43].

For a better comparison, a simulation experiment is also made and the parameters are the same as those used in the DPP-BOTDA. A 1 cm hotspot is centered in 10 m FUT, which is interrogated with a 10 ns differential pulse-phase pair. Besides, the length of the π phase-shift is 0.1 ns, corresponding to a spatial resolution of 1 cm. The power of the pump pulse is 100 mW, while it is 0.1 mW for the probe wave. The Brillouin time traces of the 10 ns (black curve) and 9.9 ns with 0.1 ns π phase pulse (red curve) are shown in figure 12, while the frequency offset between the pump and probe waves is 10.800 GHz. After the differential process, the information of the 0.1 ns π phase pulse is obtained, which is also plotted in figure 12. It can be seen that the 1 cm hotspot is clearly observed in the blue curve, and the power of the differential Brillouin signal is about twice as much as that of the DPP-BOTDA one in figure 9. Because the π phase pulse has an out-of-phase quenching effect on the acoustic wave, which is more effective than the absence of the pump wave. Therefore, the SNR of BEDS is enhanced twice compared with the DPP technique for the same spatial resolution, resulting in a better measurement accuracy.

The 3D BGSs of the BEDS are shown in figure 13(a) and the BGSs inside and outside the hotspot are presented in figure 13(b). It can be seen that the secondary echo (i.e. residual peak) is eliminated by the differential pulse-phase pair technique. The BFS difference between the BGSs inside and outside the hotspot is exactly 100 MHz, which is 10.900 GHz and 10.800 GHz, respectively. Besides, the FWHM of the

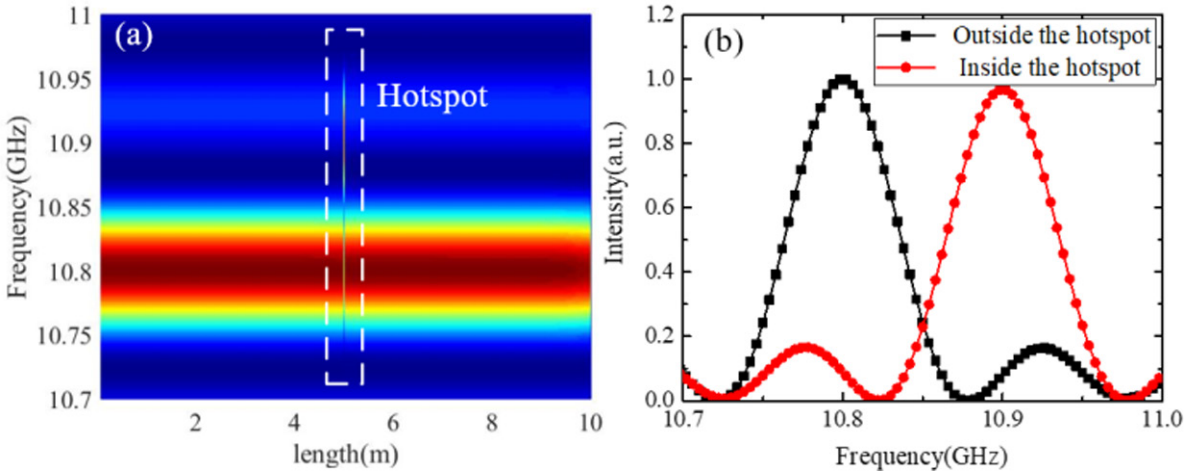

Figure 13. (a) The 3D BGSs of the BEDS along the FUT, and (b) the BGSs inside and outside the hotspot.

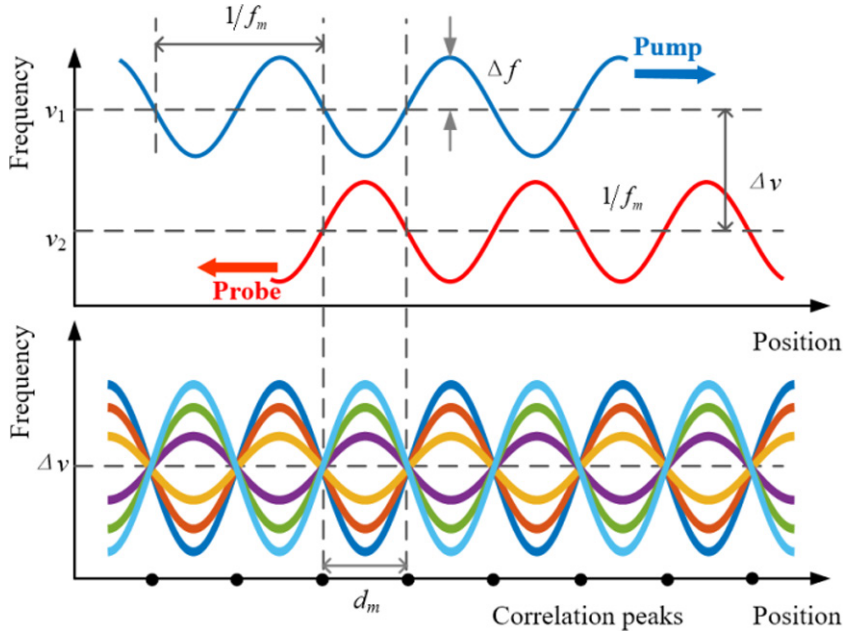

Figure 14. The operating principle of the frequency modulation-based BOCDA.

measured BGS is about 97 MHz, which is determined by the long duration pulses. And the side lobe is also measured, attributed to the pump contribution on the Brillouin spectrum. As a result, the BEDS is also a promising tool for a high-spatial-resolution Brillouin sensing, especially suitable in mid-to-long distances.

4. The developments of high-spatial-resolution BOCDA

In order to circumvent the spatial resolution limit of the pulse-based scheme, a novel technique has been proposed by using the correlation between the pump and probe waves. The SBS interaction is generated at the position with a high correlation (i.e. correlation peak), while it is suppressed outside the correlation peak. The correlation peak can be obtained by several specific modulation methods, which are the frequency modulation [7], phase modulation [19], amplified spontaneous emission [20] and chaotic laser [21]. Here, the main developments and breakthroughs are introduced about the frequency modulation and phase modulation-based BOCDA.

4.1. The frequency modulation-based BOCDA

In 1999, the correlation-based technique has been proposed to interrogate the Brillouin gain spectrum, which is enabled by the frequency modulated pump and probe waves [44]. Besides, a 45 cm resolution is demonstrated, which overcomes the obstacles for the conventional pulse-based technique. The operating principle of the frequency modulation-based BOCDA is illustrated in figure 14. In order to obtain a high correlation, the pump and probe waves are sinusoidal frequency modulated at the frequency f_m with a modulation amplitude Δf. The pump and probe waves are counter-propagating, and the frequency difference between these two waves is only fixed at the correlation peaks. In this case, the Brillouin interaction is

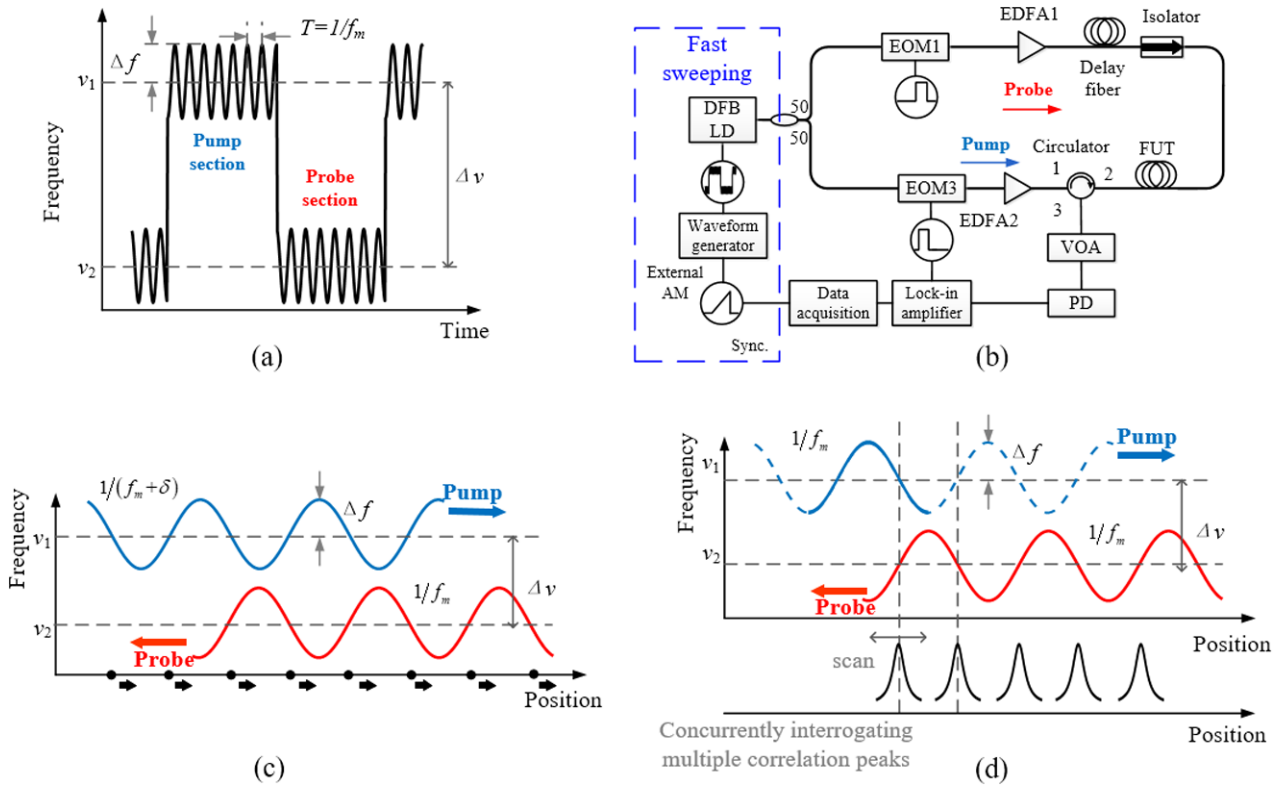

Figure 15. (a) Operating principle of a simplified BOCDA with time-division generation of pump-probe waveform; (b) experiment setup for simplified BOCDA measurement at 1 kHz sampling rate; (c) automatic sweep of the correlation peak based on the differential frequency modulation technique; and (d) BOCDA enhanced by time-domain data processing for concurrent interrogation of multiple sensing points.

constant and steady, so that there is no broadening effect on the BGS. Meanwhile, it is able to map the BGS by scanning the frequency offset between the pump and probe waves. At other positions, the frequency of the pump wave changes continuously relative to the probe wave, resulting in a suppression of the Brillouin interaction.

For this technique, the spatial resolution (Δz) is determined by the width of the correlation peak, while the measurement range (d_{m}) is limited by the interval of the correlation peaks [45]:

$$\Delta z = \frac{c}{n} \cdot \frac{\Delta v_{\mathrm{B}}}{2\pi f_{\mathrm{m}} \cdot \Delta f} \tag{7}$$

$$d_{\mathrm{m}} = \frac{c}{n} \cdot \frac{1}{2f_{\mathrm{m}}}. \tag{8}$$

In general, the non-zero peak is utilized to interrogate the FUT, the order of which is selected with a delay fiber. Therefore, the distributed measurement is enabled by changing the frequency f_{m}, as the interval of the correlation peaks is dependent on the frequency f_{m}. To obtain an ultra-high spatial resolution (1.6 mm) [22], the modulation frequency f_{m} is varying from 19.4 MHz to 19.5 MHz depending on the measurement position, while the amount of Δf is increased to 33 GHz. Here, the amplitude of the frequency modulation is much larger than the fiber BFS, resulting in a spectral overlapping between the pump and probe waves. In order to remove the pump reflection on the probe wave, a well-designed beat lock-in detection is introduced, where choppers are applied two times to pump and probe waves at different frequencies, and only one lock-in amplifier is used at the beat frequency of them.

In addition, numerous impressive techniques have been introduced into the frequency modulation-based BOCDA to enhance the sensing performance. In the conventional scheme, the laser diode (LD) is direct current modulated with a dozen megahertz sinusoidal-wave signal. Then, the frequency offset between the pump wave and probe wave is scanned with a sideband generation technique, which is realized with an MZM and a microwave generator. In order to reduce the cost and complexity, a simplified BOCDA has been proposed to generate the pump and probe waves in a time-division manner [46], where a sinusoidal-wave signal is mixed with a rectangular-wave signal as shown in figure 15(a). For measuring the BGS, the optical wave is divided into two, one of which is delayed and operated as the probe wave. Besides, the frequency offset between the pump wave and probe wave is scanned by varying the amplitude of the rectangular wave. The simplified BOCDA is a cost-effective scheme, and moreover it owns a potential of a dynamic measurement by expediting the frequency sweeping process. The sampling rate of the conventional BOCDA and BOTDA is limited by the maximum sweeping rate of a common microwave generator (<100 Hz), while it is replaced by a direct frequency modulation of the LD in the simplified BOCDA. The experiment setup of the fast simplified BOCDA [47] is shown in figure 15(b), where a waveform generator is used to generate the waveform at 100 kHz and the amplitude of the waveform is controlled by an external AM source. The BGS is mapped with 100 data

points, so that a sampling rate of 1 kHz is obtained for interrogating a single position. It can be seen that there still exists a major challenge for the fast-distributed measurement, as the modulation frequency needs to be swept. In order to solve this problem, an upgraded simplified BOCDA has been proposed based on the differential frequency modulation [48]. The sensing position is automatically and periodically swept along the FUT by applying the slightly different modulation frequencies to the pump and probe waves, as shown in figure 15(c). In the experiment, the distributed mapping of the BFS variations along a 100 m FUT is obtained with 20 Hz sampling rate and 80 cm spatial resolution. In 2018, an ultrahigh-speed BOCDA has been demonstrated with a single position of 200 kHz and a spatial resolution of 8 cm [23]. In their scheme, a data subtraction scheme is used instead of the lock-in amplifier detection, removing the measurement speed limitation of the lock-in amplifier. Besides, a voltage-controlled oscillator is utilized to fast sweep the frequency offset between the pump and probe, and the correlation peaks is scanned during the frequency-sweeping process. For a 200-position distributed measurement, a sampling rate of 1 kHz has been achieved [23].

Another main obstacle that limits the sensing performance of the BOCDA is the trade-off between the spatial resolution and the measurement range. Maintaining a high spatial resolution, the measurement range has been enlarged by several effective methods, including the double modulation [49], temporal gating [50], differential measurement [51] and time-domain data processing (i.e. time-multiplexing technique) [52]. Furthermore, by applying the double modulation and optical time gate based on the differential measurement scheme [53], a distributed strain and temperature sensing is realized with a spatial resolution of less than 1 cm over 10.5 km FUT, which effectively resolves more than 1 million sensing points. However, it will take more than 231 d to interrogate all of the 1 million sensing points, which seriously deteriorates the practicality of the sensor. One of the effective solutions is the time-domain data processing, and its schematic diagram is shown in figure 15(d), where the frequency-modulated pump wave is simultaneously pulse modulated. Therefore, it is capable of concurrently interrogating multiple correlation peaks along the FUT. It should be noted that the measurement range is enlarged with no sacrifice of the measurement time. In the experiment, 148 correlation peaks are simultaneously measured with a spatial resolution less than 3 cm along 1530 m FUT. However, each correlation peak is still required to interrogate hundreds of positions, which is ultimately limited by the range between two adjacent correlation peaks (d_m). Besides, it is impractical to reduce the d_m drastically by increasing the f_m. In summary, the frequency modulation-based BOCDA can provide a cost-effective sensing scheme, owning the capability of a high spatial resolution, high speed and more than 1 million effective sensing points.

4.2. The phase modulation-based BOCDA

In 2012, another type of the CW-based BOCDA has been realized with the optical phase modulation technique [19]. It is able to decouple the connection between the spatial resolution and measurement range, which mainly limits the sensing performance of the frequency modulation-based BOCDA. The operating principle of the phase modulation-based BOCDA is illustrated in figure 16, where the pump and probe waves are simultaneously modulated by a high-rate pseudo random bit sequence (PRBS). The modulation phase within each symbol is a value of either 0 or π with equal probabilities, and moreover the duration of each bit (t_d) is much shorter than the acoustic wave lifetime. Within the correlation peak, the phase difference between the pump wave and probe wave is fixed, so that the acoustic wave is built up and kept at a steady state. In other positions, the acoustic wave is randomly alternating between the state of being excited and quenched, resulting in a zero expectation value. Similar to the frequency modulated BOCDA, the SBS interaction is only generated at the correlation peak.

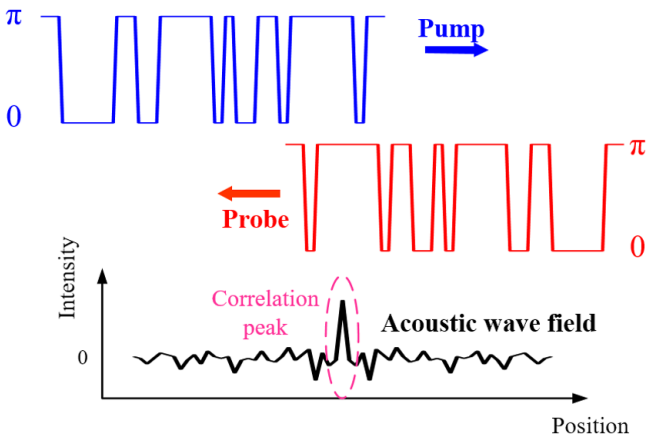

Figure 16. The operating principle of the phase modulation-based BOCDA.

In addition, the spatial resolution (Δz) and the measurement range (d_m) is also determined by the width of the correlation peak and the interval of the correlation peaks, respectively.

$$\Delta z = \frac{c}{n} \cdot \frac{t_d}{2} \tag{9}$$

$$d_m = M \cdot \frac{c}{n} \cdot \frac{t_d}{2} \tag{10}$$

where M is the number of codes and t_d is the duration of one code. Meanwhile, the M should be sufficiently big to guarantee only one correlation peak within the FUT. For a distributed sensing, the high-order correlation peak is scanned along the FUT through a slight change on the PRBS symbol duration.

However, two main issues need to be addressed, which limit the sensing performance of this type of BOCDA. One is the residual off-peak Brillouin interaction, the instantaneous value of which is nonzero and fluctuating. This interaction accumulates over the entire length of the FUT, which is regarded as the noise of the measurements. Therefore, a large number of averaging is required to enhance the SNR. In 2013, the off-peak interaction is significantly reduced by using an intensity-modulated pump wave and time-gated detection [54], as the noise is only introduced inside the time gate. The other is that tens of thousands of positions need to be interrogated for a distributed measurement, which is an extremely

time-consuming process. In 2014, an important development towards the high-resolution and long-range BOCDA has been made by combining the time-domain and correlation-domain analysis, known as the time-multiplexing BOCDA [55]. In this scheme, the pump wave is also pulse modulated to reduce the noise and, at the same time, a large number of correlation peaks are generated in the FUT. The SBS interaction at different peaks can be temporally resolved, resulting in a simultaneous measurement at multiple correlation peaks. In this case, the BGS is mapped along a 400 m FUT with a spatial resolution of 2 cm (i.e. 20 000 effective sensing points), while the measurement time is saved by a factor of over 150 as every correlation peak only interrogates 127 positions. To excite the acoustic wave to a steady state, the pulse width should be no less than 30 ns, so that hundreds of interrogated positions is still required in the measurement. In 2016, the DPP acquisition is combined with the time-multiplexing to further reduce the necessary number of interrogated positions by an order of magnitude [56]. Therefore, the minimum separation between adjacent correlation peaks is equal to the difference of the pulse-width pair, which is much shorter than the duration of a single pulse and even shorter than the acoustic wave lifetime. Compared with the frequency modulation-based BOCDA, the DPP technique allows the phase modulation-based BOCDA to further reduce the interrogated positions, resulting in a drastically reduction on the measurement time. Besides, a short perfect Golomb code can be used instead of the PRBS, which is able to effectively reduce the coding noise [55, 56].

Based on a detailed theoretical analysis of the system limitations and an optimization process with the best SNR, a record-high number of 2 100 000 has been achieved with the temporal gating technique and time-domain acquisition [24]. In addition, another source of noise induced by the non-instantaneous phase transitions has been reported, which is introduced by the device bandwidth limitation in the phase modulation. This noise has a negative effect on the sensor performance, especially detrimental to obtain an ultra-high spatial resolution.

Recently, we have made some work to eliminate the bit transition edge induced noise by using the phase-shift-keying technique, which only generates two phase shifts (0 and π) for phase coding using an MZM [57]. This phase coding technique is not sensitive to the bandwidth of the related equipment. A PRBS phase coding with 20 ps bit duration without transition edge is realized with a 50 GS/s AWG in the proposed BOCDA based on the phase-shift-keying technique. In order to verify its spatial resolution, two fiber segments with different BFS are spliced together for test. For a distributed measurement, the correlation peak is scanned with a moving step of 0.4 mm. A 2 mm transition region with two Brillouin peaks is measured, which is caused by the finite spatial resolution of the proposed sensor. In turn, the 2 mm spatial resolution of the proposed sensor is validated by the length of the transition region.

5. Discussions and conclusions

The Brillouin-based optical fiber sensors have been extensively studied in the last two decades, and they are good solutions to the structure health monitoring and intelligent urban data collecting. In this paper, a brief overview of the developments on the high-spatial resolution BOTDA and BOCDA is made. In the BOTDA scheme, several impresssive techniques have been proposed for a centimeter spatial resolution, including the dark-pulse technique, PPP technique, DPP technique and Brillouin echo technique. For the dark-pulse and PPP techniques, the non-local information is introduced into the Brillouin spectrum, which is distorted at small temperature and strain variations, resulting in a system error. The DPP and Brillouin echo techniques utilize the differential measurements with two pump pulses, and these two types of sensors are free from this problem. Besides, the intensity of BEDS differential signal is twice as much as that of the DPP one, when using the same experimental parameters. Therefore, the BEDS owns a better SNR and measurement accuracy, which manifests itself as a promising tool to achieve a high spatial resolution in mid-to-long distances. Meanwhile, the DPP-BOTDA has also been widely used in the laboratory investigations and practical applications, as the implementation is simple and easy. The best spatial resolution of the DPP-BOTDA and BEDS is ultimately limited by the bandwidth of the pulse generator and the detection system. Aiming at a high spatial resolution, the other improvements of the BOTDA sensors are also pursued, such as the sensing range and measurement accuracy. In the BOCDA scheme, it is able to circumvent the pulse-based spatial resolution limit and spatial resolution is determined by the width of the correlation peak. For the frequency modulation BOCDA, an ultra-high spatial resolution of 1.6 mm is achieved with a dozen megahertz sinusoidal-wave signal, while it requires tens of gigahertz random modulation in the frequency modulation-based BOCDA sensors. Moreover, the sensor performance is also enhanced in the aspect of system simplification, fast measurement, enlarging the sensing range and so on. The phase modulation based BOCDA is able to decouple the connection between the spatial resolution and measurement range. By combining with the time-multiplexing technique, it is able to realize the simultaneous measurement at multiple correlation peaks, so that the time-multiplexing BOCDA offers a promising solution to a high-spatial-resolution and long-range Brillouin sensing. After an optimization process, a spatial resolution of 8.3 mm is realized over 17.5 km sensing fiber, resulting in a record-high number of 2 100 000 resolving points. Recently, the bit transition edge induced noise has been eliminated by using the phase-shift-keying technique, so that an ultra-high spatial resolution of 2 mm is obtained. Furthermore, a spatial resolution of 0.5 mm has been reported using an ASE light source in the BOCDA scheme, which can detect feature sizes down to 0.2 mm on a silicon-chalcogenide photonics waveguide [58]. In conclusion, the BOTDA and BOCDA sensors are able to realize a high spatial resolution of centimeters and even millimeters, which have broad prospects in the practical applications.

The main challenges and improvements remain as follows:

(1) Introduce the advanced algorithms to break the device bandwidth limitation, and then further improve the spatial resolution of the BOTDA and BOCDA sensors.

(2) In the phase modulation-based BOCDA, the bit transition-edge-induced noise has been eliminated by using the phase-shift-keying technique, and therefore, more research work is expected to comprehensively upgrade the sensing performance.
(3) To obtain a high-spatial resolution, the cost, stability and simplicity of the system should be also considered, which is equally important in the practical applications.

Acknowledgments

This work was supported by the National Key Scientific Instrument and Equipment Development Project of China, Grant No. 2017YFF0108700 and National Natural Science Foundation of China, Grant No. 61575052.

ORCID iDs

Benzhang Wang https://orcid.org/0000-0003-0739-7832
Yongkang Dong https://orcid.org/0000-0001-8985-9310

References

[1] Horiguchi T, Shimizu K, Kurashima T, Tateda M and Koyamada Y 1995 Development of a distributed sensing technique using Brillouin scattering *J. Lightwave Technol.* **13** 1296–302
[2] Zhang H, Zhou D, Wang B, Pang C, Xu P, Jiang T, Ba D, Li H and Dong Y 2018 Recent progress in fast distributed Brillouin optical fiber sensing *Appl. Sci.* **8** 1280
[3] Diakaridia S, Pan Y, Xu P, Zhou D, Wang B, Teng L, Lu Z, Ba D and Dong Y 2017 Detecting cm-scale hot spot over 24 km-long single-mode fiber by using differential pulse pair BOTDA based on double-peak spectrum *Opt. Express* **25** 17727–36
[4] Alahbabi M N, Cho Y T and Newson T P 2006 Long-range distributed temperature and strain optical fibre sensor based on the coherent detection of spontaneous Brillouin scattering with in-line Raman amplification *Meas. Sci. Technol.* **17** 1082
[5] Soto M A, Bolognini G, Pasquale D P and Thevenaz L 2010 Long-range Brillouin optical time-domain analysis sensor employing pulse coding techniques *Meas. Sci. Technol.* **21** 094024
[6] Xu J, Dong Y, Zhang Z, Li S, He S and Li H 2016 Full scale strain monitoring of a suspension bridge using high performance distributed fiber optic sensors *Meas. Sci. Technol.* **27** 124017
[7] Hotate K and Tanaka M 2002 Distributed fiber Brillouin strain sensing with 1 cm spatial resolution by correlation-based continuous-wave technique *IEEE Photonics Technol. Lett.* **14** 179–81
[8] Bao X, Brown A, DeMerchant M and Smith J 1999 Characterization of the Brillouin-loss spectrum of single-mode fibers by use of very short (<10 ns) pulses *Opt. Lett.* **24** 510–12
[9] Brown A, DeMerchant M, Bao X and Bremner T 1998 Advances in distributed sensing using Brillouin scattering *Proc. SPIE* **3330** 294–300
[10] Afshar S, Ferrier G, Bao X and Chen L 2003 Effect of the finite extinction ratio of EOM on the performance of the pump-probe Brillouin sensor system *Opt. Lett.* **28** 1418–20
[11] Brown A W, Colpitts B G and Brown K 2005 Distributed sensor based on dark-pulse Brillouin scattering *IEEE Photonics Technol. Lett.* **17** 1501–3
[12] Kishida K, Li C and Nishiguchi K 2005 Pulse pre-pump method for cm-order spatial resolution of BOTDA *Proc. SPIE* **5855** 559–62
[13] Li W, Bao X, Li Y and Chen L 2008 Differential pulse-width pair BOTDA for high spatial resolution sensing *Opt. Express* **16** 21616–25
[14] Dong Y, Zhang H, Chen L and Bao X 2012 2 cm spatial-resolution and 2 km range Brillouin optical fiber sensor using a transient differential pulse pair *Appl. Opt.* **51** 1229–35
[15] Dominguez-Lopez A, Soto M A, Martin-Lopez S, Thevenaz L and Gonzalez-Herraez M 2017 Resolving 1 million sensing points in an optimized differential time-domain Brillouin sensor *Opt. Lett.* **42** 1903–6
[16] Foaleng S M, Tur M, Beugnot J C and Thevenaz Luc 2010 High spatial and spectral resolution long-range sensing using Brillouin echoes *J. Lightwave Technol.* **28** 2993–3003
[17] Song K Y, Chin S, Primerov N and Thevenaz L 2010 Time-domain distributed fiber sensor with 1 cm spatial resolution based on Brillouin dynamic grating *J. Lightwave Technol.* **28** 2062–6
[18] Chao J, Wen X, Zhu W, Min L, Lv H and Kai S 2019 Subdivision of Brillouin gain spectrum to improve the spatial resolution of a BOTDA system *Appl. Opt.* **58** 466–72
[19] Zadok A, Antman Y, Primerov N, Denisov A, Sancho J and Thevenaz L 2012 Random-access distributed fiber sensing laser *Photonics Rev.* **6** L1–5
[20] Cohen R, London Y, Antman Y and Zadok A 2014 Brillouin optical correlation domain analysis with 4 millimeter resolution based on amplified spontaneous emission *Opt. Express* **22** 12070–8
[21] Zhang J, Feng C, Zhang M, Liu Y, Wu C and Wang Y 2018 Brillouin optical correlation domain analysis based on chaotic laser with suppressed time delay signature *Opt. Express* **26** 6962–72
[22] Song K Y, He Z and Hotate K 2006 Distributed strain measurement with millimeter-order spatial resolution based on Brillouin optical correlation domain analysis and beat lock-in detection scheme *18th Int. Conf. Optical Fiber Sensors* (https://doi.org/10.1364/OFS.2006.ThC2)
[23] Wang B, Fan X, Fu Y and He Z 2018 Dynamic strain measurement with kHz-level repetition rate and centimeter-level spatial resolution based on Brillouin optical correlation domain analysis *Opt. Express* **26** 6916–28
[24] Denisov A, Soto M A and Thevenaz L 2016 Going beyond 1000 000 resolved points in a Brillouin distributed fiber sensor: theoretical analysis and experimental demonstration *Light Sci. Appl.* **5** e16074
[25] Boyd R W 2008 *Nonlinear Optics* 3rd edn (New York: Academic) pp 429–47
[26] Kobyakov A, Sauer M and Chowdhury D 2010 Stimulated Brillouin scattering in optical fibers *Adv. Opt. Photonics* **2** 1–59
[27] Bao X and Chen L 2011 Recent progress in Brillouin scattering based fiber sensors *Sensors* **11** 4152–87
[28] Chu R, Kanefsky M and Falk J 1992 Numerical study of transient stimulated Brillouin scattering *J. Appl. Phys.* **71** 4653–8
[29] Soto M A and Thevenaz L 2013 Modeling and evaluating the performance of Brillouin distributed optical fiber sensors *Opt. Express* **21** 31347–66

[30] Brown A W, Colpitts B G and Brown K 2007 Dark-pulse Brillouin optical time-domain sensor with 20 mm spatial resolution *J. Lightwave Technol.* **25** 381–6
[31] Lecoeuche V, Webb D J, Pannell C N and Jackson D A 2000 Transient response in high-resolution Brillouin-based distributed sensing using probe pulses shorter than the acoustic relaxation time *Opt. Lett.* **25** 156–8
[32] Cho S B, Lee J J and Kwon B II 2006 Pulse base effect on the strain measurement of a Brillouin-scattering-based distributed optical fiber sensor *Smart Mater. Struct.* **15** 315–24
[33] Kishida K and Li C H 2005 Pulse pre-pump-BOTDA technology for new generation of distributed strain measuring system *Structural Health Monitoring and Intelligent Infrastructure* vol 1 (London: Taylor & Francis) pp 471–7 (http://www.shashiya.com/produce/PPPBOTDA.pdf)
[34] Wang F, Bao X, Chen L, Li Y, Snoddy J and Zhang X 2008 Using pulse with a dark base to achieve high spatial and frequency resolution for the distributed Brillouin sensor *Opt. Lett.* **33** 2707–9
[35] Jamioy C A G and Lopez-Higuera J M 2011 Decimeter spatial resolution by using differential preexcitation BOTDA pulse technique *IEEE sens. J.* **11** 2344–8
[36] Li Y, Bao X, Dong Y and Chen L 2010 A novel distributed Brillouin sensor based on optical differential parametric amplification *J. Lightwave Technol.* **28** 2621–6
[37] Dominguez-Lopez A, Yang Z, Soto M A, Angulo-Vinuesa X, Martin-Lopez S, Thevenaz L and Gonzalez-Herraez M 2016 Novel scanning method for distortion-free BOTDA measurements *Opt. Express* **24** 10188–204
[38] Wang B, Fan B, Zhou D, Pang C, Li Y, Ba D and Dong Y 2019 High-performance optical chirp chain BOTDA by using a pattern recognition algorithm and the differential pulse-width pair technique *Photonics Res.* **7** 652–8
[39] Urricelqui J, Sagues M and Loayssa A 2015 Brillouin optical time-domain analysis sensor assisted by Brillouin distributed amplification of pump pulses *Opt. Express* **23** 30448–58
[40] Mompo J J, Urricelqui J and Loayssa A 2016 Brillouin optical time-domain analysis sensor with pump pulse amplification *Opt. Express* **24** 12672–81
[41] Thevenaz L and Mafang S F 2008 Distributed fiber sensing using Brillouin echoes *Proc. SPIE* **7004** 70043N
[42] Beugnot J C, Tur M, Mafang S F and Tevenaz L 2011 Distributed Brillouin sensing with sub-meter spatial resolution: modeling and processing *Opt. Express* **19** 7381–97
[43] Lee M W, Stiller B, Hauden J, Mailotte H, Roch C, Tevenaz L and Sylvestre T 2012 Differential phase-shift-keying technique-based Brillouin echo-distributed sensing *IEEE Photonics Technol. Lett.* **14** 179–81
[44] Hotate K and Hasegawa T 1999 Measurement of Brillouin gain spectrum distribution along an optical fiber with a high spatial resolution using a novel correlation-based technique: demonstration of 45cm spatial resolution *13th Int. Conf. Optical Fiber Sensors* vol W3-3 pp 337–40
[45] Song K Y and Hotate K 2006 Enlargement of measurement range in a Brillouin optical correlation domain analysis system using double lock-in amplifiers and a single-sideband modulator *IEEE Photonics Technol. Lett.* **3** 499–501
[46] Hasegawa T and Hotate K 1999 Measurement of Brillouin gain spectrum distribution along an optical fiber by direct frequency modulation of a laser diode *Proc. SPIE* **3860**
[47] Song K Y and Hotate K 2007 Distributed fiber strain sensor with 1 kHz Sampling rate based on Brillouin optical correlation domain analysis *IEEE Photonics Technol. Lett.* **19** 1928–30
[48] Song K Y, Kishi M, He Z and Hotate K 2011 High-repetition-rate distributed Brillouin sensor based on optical correlation-domain analysis with differential frequency modulation *Opt. Lett.* **36** 2062–4
[49] Mizuno Y, He Z and Hotate K 2010 Measurement range enlargement in Brillouin optical correlation-domain reflectometry based on double-modulation scheme *Opt. Express* **18** 5926–33
[50] Yamashita R K, Zou W, He Z and Hotate K 2012 Measurement Range Elongation Based on Temporal Gating in Brillouin Optical Correlation Domain Distributed Simultaneous Sensing of Strain and Temperature *IEEE Photonics Technol. Lett.* **24** 1006–8
[51] Jeong J H, Lee K, Song K Y, Jeong J M and Lee S B 2012 Differential measurement scheme for Brillouin optical correlation domain analysis *Opt. Express* **20** 27094–101
[52] Ryu G, Kim G T, Song K Y, Lee S B and Lee K 2017 Brillouin optical correlation domain analysis enhanced by time-domain data processing for concurrent interrogation of multiple sensing points *J. Lightwave Technol.* **35** 5311–6
[53] Kim Y H, Lee K and Song K Y 2015 Brillouin optical correlation domain analysis with more than 1 million effective sensing points based on differential measurement *Opt. Express* **23** 33241–8
[54] Denisov A, Soto M A and Thevenza L 2013 Time gated phase-correlation distributed Brillouin fibre sensor *Proc. SPIE* **8794** 87943I
[55] Elooz D, Antman Y, Levanon N and Zadok A 2014 High-resolution long-reach distributed Brillouin sensing based on combined time-domain and correlation-domain analysis *Opt. Express* **22** 6453–63
[56] Shlomi O, Preter E, Ba D, London Y, Antman Y and Zadok A 2016 Double-pulse pair Brillouin optical correlation-domain analysis *Opt. Express* **24** 26867–76
[57] Ba D, Li Y, Zhang X, Yan J and Dong Y 2019 Phase-coded Brillouin optical correlation domain analysis with 2 mm resolution based on phase-shift keying *Opt. Express* **27** 36197–205
[58] Zarifi A *et al* 2019 On-chirp correlation-based Brillouin sensing: design, experiment, and simulation *J. Opt. Soc. Am.* B **57** 146–52